The Characteristics and Microstructure of PV Degradation

Tanokkorn Chenvidhya[1], Sirinuch Chindaruksa[2], Chatchai Sirisamphanwong[2],
and Buntoon Wiengmoon[2,*]

ARTICLE INFO

ABSTRACT

This aims to study the degradation-rated PV cells of the electrical characteristic. The over 15 years old of PV module is used as the sample of the test. It is 53 Wp of mono-crystalline silicon (mono-c-Si) PV module. A comprehensive analysis of the relationship between the physical and electrical parameters of a cell degradation rate on the module is carried out. The degraded PV modules involve a decrease in natural aging and severe degradations. For PV serious degradation regarding the amount of EVA delamination and corrosion on the busbar. The I-V attribute was tested at 1000 W/m2 irradiance with 1.5 air mass and 25 oC module temperature. Moreover, the defect of microstructure and quantity of delamination on cells were investigated using Image J and SEM. The electrical parameters specify that the degradation-rated maximum power output (Pm) and fill factor (FF) are about 52% and 43%, subsequently. The degradation-rated short-circuit current is about 15%. Incidentally, degradation-rated open-circuit voltage is sameness. Furthermore, the parasitic parameter is related to the value of the photocurrent (Iph) in agreement with the short-circuit current which the current generation of the module has decreased. The saturation current density (I0), and ideality factor (n) are reduced due to an increasing degradation-rated short-circuit current. High-level series resistance (Rs) and low-level shunt resistance (Rsh) due to the degradation-rated maximum power output and fill factor are increased. The physical parameter of PV module results indicates that EVA delamination is no effect on the current generation. The sunlight can travel into the cell although the delamination of EVA. Using the SEM method, the cell of the module shows a green patina and black color on the busbar.

1. INTRODUCTION

Renewable energy is clean energy that humans create from natural resources to utilize for a comfortable life and clean environment, for instance, sunlight, and wind.

Their availability relies on the season and daytime challenge controllable and generally call intermittent. However, it is constantly evolving. The advantage of the inexhaustible, and distribution of growth of green electricity worldwide as well as the high performance of solar energy technologies will provide long-term benefits [1]. Photovoltaic systems are the most important renewable energy generation. Solar radiation is converted to electricity using photovoltaic cells [2,3]. Annual global solar system growth in 2020 will gain 142 GW. Increasing 14 % over the prior year. Investors in PV systems mention the reliability of field operations and endurance as the terms of warranty conditions which is significant to the perception of reality to benefit of investment return. Meanwhile, manufacturers of PV module attempt to persuade customers by providing warranties for their modules [4]. The reliability and lifetime of such PV systems need to be comprehensively understood. Generally, decreasing PV module output along the time of field operation is wherewith the aging of materials and its part of the device. The PV module lifetime is estimated at 20 years and more than 25 years. Moreover, service life goes toward the warranty of the manufacturers' initial value of maximum power output less than 90 % of a decade and 80 % of 25 years of field operation. The rated power output for crystalline silicon PV modules reduces by 0.8 %/year. Nevertheless, manufacturers are foraging to prolong the life warranty duration to 30 years, indicating a reduction of the highest annual performance by barely 0.65% [4,5]. Previous studies have reported the monitoring of characteristics of PV module degradation in field operations which are factors of PV module defect affecting the durability of the interfaces in the module including ultraviolet light, ambient temperature, and humidity of the environment. Examples of PV module defects are discoloration and delamination of

[1]*CES Solar Cells Testing Center (CSSC), King Mongkutt University, Thailand.*
[2]*Department of Physics, Faculty of science, Naresuan University, Phitsanulok, Thailand.*
*Corresponding author: Buntoon Wiengmoon; Phone: +66-5-596-3513; Fax: +66-5-596-3501; E-mail: buntoonw@nu.ac.th.

encapsulated material of PV modules, as well as the air bubble on the backsheet, both cell cracks, and microcracks, burnt at the cell area due to the hotspot, and defect of the anti-reflective coating, etc [6]. The degradation mechanism in the field operation could explain the reliability of the long period of the PV module operation. The reliability concern and degradation of performance may cause by the aging of and adhesion loss of encapsulant and semiconductor materials, also the solar cell interconnection [7]. All concerns involved in the reliability of PV modules in long term are particularly vital. The International Electro-Technical Commission (IEC) provides the qualification standard, such as IEC61215, for wafer-based crystalline Si modules, and IEC 61646, for thin-film modules, as well as the safety standard IEC61730, to encourage securing the PV modules to high reliability [8]. So, the inquisition of failure and deterioration of PV modules has gained a significant concern because reliability and service life are important issues in-field performance and conditions of the warranty [9]. Therefore, this work aims to investigate the microstructure of aged PV panels that have several degradations. The severe degradation PV panel was analyzed for the panel's I-V characteristics and the build-in PV cell of No. 1 to 36 cells. The degradations of I_{sc}, V_{oc}, P_m, and FF were analyzed. Finally, the physical analysis of the EVA delamination and microstructure on the busbar was studied.

2. I-V CHARACTERISTIC AND MATHEMATICAL MODEL

The photovoltaic module composes of cells that are weaved in series. A Typical I-V plot is a PV module's electrical characteristic. The set of current and voltage values are plotted as an I-V curve directly that is calculated and plotted as a P-V curve, which is shown in Fig.1. These obtain from PV tracers that are measuring both the current and voltage at multiple points and can apply to the module and the string measurement. The fundamental parameters include (1) the initial points namely the short-circuit current (I_{sc}), and the open-circuit voltage (V_{oc}), and (2) the highest points are the current at maximum power point (I_{mp}), the voltage at maximum power point (V_{mp}), as well as the maximum output power (P_m).

Typically, an equivalent circuit of a diode as shown in Fig.2. can be expressed mathematical model by equation (1). Explainable of a Shockley's diode that is weaved in parallel to the current source, the shunt resistant (R_{sh}) while connect in series with the resistant (R_s) and the load. Equation (1) consists of the photocurrent (I_{ph}), this current will be a loss of flows through the diode (I_d) and flows through a parallel resistance current (I_{sh}). There was reduced by current generate. Substituting in for the values of I_d and I_{sh} is shown in equation (1). Important parameters consist of the resistance of connection or series resistance (R_s), resistance from material quality namely shunt resistance

(R_{sh}), the photocurrent (I_{ph}), the saturation current density (I_0), and the ideality factor (n).
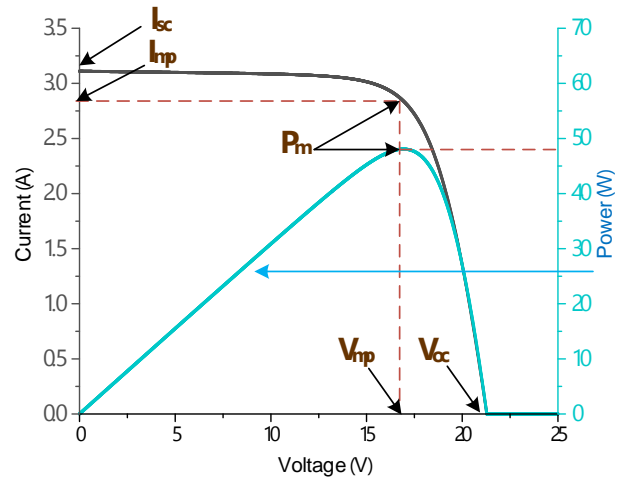

Fig. 1. Typical of current and voltage (I-V) and power and voltage (P-V) curves.
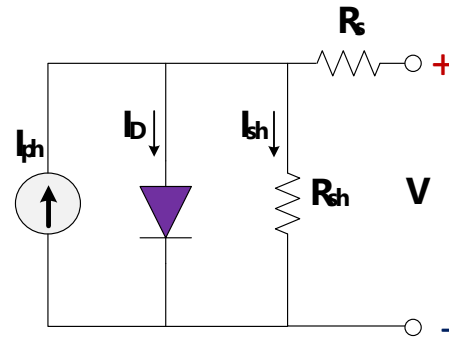

Fig. 2. The Equivalent Circuit of a PV Cell.

$$I = I_{ph} - I_D - I_{sh} = I_{ph} - I_0 \left\{ \exp\left(\frac{q(V + IR_s)}{nkTN_s} \right) - 1 \right\} - \frac{V + IR_s}{R_{sh}} \quad (1)$$

where, I is the current of PV module output in amperes (A), V is the voltage of PV module output in volts (V), q is the charge of an electron equal to $1.602176634 \times 10^{-19}$ C, k is Boltzmann's constant equal to 1.380649×10^{-23} J/K, N_s is the total number of cells in series, and T is the standard temperature at STC equal to 298.15 K.

3. MEASUREMENT APPARATUS AND PROCEDURE

The experiment is carried out in this work using the mono-c-si PV modules 53 Wp, of 36 cells in series, size 104.04 cm^2 of the area as in Fig.3), the PV module was operating in field conditions for over 15 years old. In this research, the module, which has a natural degradation and severe degradation is selected to measure the I-V characteristics under standard test conditions (STC) at 1000 W/m^2,

temperature 25 °C, Spectral distribution of irradiance AM1.5 according to IEC 60904 [10]. To compare I-V characteristics and degradation rate analysis between natural degradation and severe degradation. Then, a module of severe degradation carried out I-V characteristics measurements under the STC condition of each cell and describes a variety of EVA delamination. After that, to describe microstructural defects in crystalline silicon solar cells which appear during the cells. The details of each part show the following.

3.1 Diagram of cells testing

A diagram for measuring the electrical parameters of each cell is illustrated in Fig.3. The first cell at the positive terminal of the module, and the last cell at the negative terminal are connected, and other cells are connected in series. Then connect a wire on the negative couple busbar on their cells. I-V characteristics inspection on the positive and negative terminals on each cell on the attached wire.

Fig.3. Diagram of cells on PV module 53 Wp.

3.2 The parasitic parameter analysis

Fig. 2. shows the instance of I–V and P–V plots of a PV module in which the maximum power point (MPP) is the one peak point at the P–V curve. While the I–V curve characteristic indicates the five parameters that have the five algebraic equations, including R_s, R_{sh}, I_{ph}, I_0, and n parameters. In the same way, terms in the specification document include electrical parameters such as I_{sc}, V_{oc}, V_{mp}, and I_{mp}, these are Standard Testing Condition (STC) conditions for PV module purchasing. The STC implies 1000 W/m² of irradiance and 25 °C of PV module temperature [11]. Particularly three significant points in the I–V and P–V characteristics: the short circuit point, the open circuit point, and the MPP point are interesting. Which these the voltage (V) and current (I) values of the three points are the basic values and are consequently applied to produce pertinent equations as below:

• At the point of the short circuit that the voltage is equal to zero: $V = 0$, $I = I_{sc}$. Eq. (1) can thus be indicated as follows:

$$I_{sc} = I_{ph} - I_0\left[\exp\left(\frac{qIR_s}{nkTN_s}\right) - 1\right] - \frac{I_{sc}R_s}{R_{sh}} \quad (2)$$

• At the point of the open circuit that the current is equal to zero: $I = 0$, $V = Voc$. Substitute the values into Eq. (1) yields:

$$I_{ph} = I_0\left[\exp\left(\frac{qV_{oc}}{nkTN_s}\right) - 1\right] + \frac{V_{oc}}{R_{sh}} \quad (3)$$

Excluding the two equations above, three other equations should be composed to gain the values of the 5-parameters. The differential equation shows in Eq. (1).

$$\frac{dV}{dI} = -R_s - \frac{aR_{sh}}{a + I_0R_{sh}\exp\left(\frac{V + IR_s}{a}\right)} \quad (4)$$

where, the thermal voltage "a" is presented by $a = \frac{nkTN_s}{q}$. Substituting the values of the short circuit (0, I_{sc}) and the open circuit (V_{oc}, 0) points, into Eq. (4).

• At the short circuit point:

$$\left.\frac{dV}{dI}\right|_{V=0} = -R_s - \frac{aR_{sh}}{a + I_0R_{sh}\exp\left(\frac{I_{sc}R_s}{a}\right)} \quad (5)$$

• At the open circuit point:

$$\left.\frac{dV}{dI}\right|_{I=0} = -R_s - \frac{aR_{sh}}{a + I_0R_{sh}\exp\left(\frac{V_{oc}}{a}\right)} \quad (6)$$

Account of only a peak of a PV module output at standard test conditions (STC), resulting in the output power differential equation of the MPP being equal to zero. Accordingly,

$$\left.\frac{dP}{dV}\right|_{P=P_m} = I_m + V_m \left.\frac{dI}{dV}\right|_{P=P_m} = 0 \quad (7)$$

That is:

$$\left.\frac{dV}{dI}\right|_{P=P_m} = -\frac{V_m}{I_m} \quad (8)$$

Combining Eqs. (8) and (4) then:

$$\frac{V_m}{I_m} = R_s + \frac{aR_{sh}}{a + I_0R_{sh}\exp\left(\frac{V_m + I_mR_s}{a}\right)} \quad (9)$$

There are five algebraic equations, as equations (2), (3), (5), (6), and (9), are set, from which the 5 parameters can be calculated. A series of simply is applied, and the explicit solutions of the 5 parameters can be reached as follows:

$$R_s = \frac{V_{mp}\left(\left.\frac{dV}{dI}\right|_{I=0} - \left.\frac{dV}{dI}\right|_{V=0}\right)\left[\left.\frac{dV}{dI}\right|_{V=0}\left(I_{sc}-I_{mp}\right)+V_{mp}\right] - \left.\frac{dV}{dI}\right|_{I=0}\left[\left(\left.\frac{dV}{dI}\right|_{V=0}I_{mp}+V_{mp}\right)\left(\left.\frac{dV}{dI}\right|_{V=0}I_{sc}+V_{oc}\right)\right]}{I_{mp}\left(\left.\frac{dV}{dI}\right|_{I=0} - \left.\frac{dV}{dI}\right|_{V=0}\right)\left[\left.\frac{dV}{dI}\right|_{V=0}\left(I_{sc}-I_{mp}\right)+V_{mp}\right] + \left(\left.\frac{dV}{dI}\right|_{V=0}I_{mp}+V_{mp}\right)\left(\left.\frac{dV}{dI}\right|_{V=0}I_{sc}+V_{oc}\right)} \quad (10)$$

$$R_{sh} = -R_s - \left.\frac{dV}{dI}\right|_{V=0} \quad (11)$$

$$I_{ph} = I_{sc}\left(1+\frac{R_s}{R_{sh}}\right) \quad (12)$$

$$n = \frac{\left(\left.\frac{dV}{dI}\right|_{I=0} + R_s\right)\left(\left.\frac{dV}{dI}\right|_{V=0}I_{sc}+V_{oc}\right)}{\left(\left.\frac{dV}{dI}\right|_{I=0} - \left.\frac{dV}{dI}\right|_{V=0}\right)} \quad (13)$$

$$I_0 = \frac{\left(I_{ph}-\frac{V_{oc}}{R_{sh}}\right)}{\left(\exp\left(\frac{V_{oc}}{n}\right)-1\right)} \quad (14)$$

In Equation (10) to (14), the 5 parameters can be indicated when I_{sc}, V_{oc}, I_m, V_m, $dV/dI(V=0)$, and $dV/dI(I=0)$ are known.

3.3 The degradation rate analysis

The degradation-rated electrical parameters namely the short-circuit current, open-circuit voltage, maximum output power, as well as fill factor are calculated by the nameplate of the module, obtained from the manufacturer's specification document, and applying the following formula in the equation (15) [7]. Calculation of the lifetime can estimate by using the degradation rate follows in equation (16) [12].

$$Degradation\ rate\,(\%) = \left(\frac{IP-PAD}{IP}\right)\times 100 \quad (15)$$

$$The\ lifetime\,(year) = \frac{100\% - RD}{LD} \quad (16)$$

where, IP is the initial value of parameters, *PAD* is the parameter after degradation, *RD* is the degradation rate that its unit is in percent per year, and *LD* is the limit of degradation per year.

3.4 The EVA delamination

In this method, the percentage relative EVA delamination was analyzed by Image J with the scanning in resolution 1200 dpi. Shown in Table 1 and the calculation of the EVA delamination area, shading area, and exposure area following equations (17), (18), and (19) respectively. The EVA delamination (EVAD) showed by equation (17);
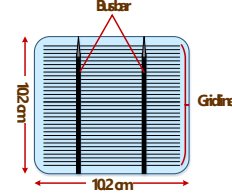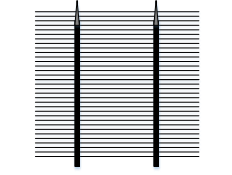
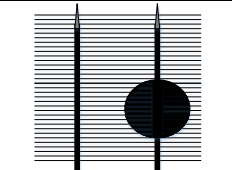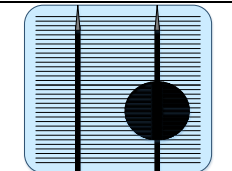$$EVAD = \frac{D}{A}\times 100 \quad (17)$$

The shading area on cell (SA) is shown by equation (18):

$$SA = \left(\frac{D - b_D g_D}{A - BG}\right)\times 100 \quad (18)$$

Calculation of Exposure area on cell (EA) shown by equation (19):

$$EA = \left(\frac{A - BG - D - b_D g_D}{A - BG}\right)\times 100 \quad (19)$$

Table. 1. Definition for analysis of cell area

Characteristics	Signification	Abbreviation
	The area of the cells (size 104.04 cm^2)	A
	The area of the busbar gridline of a cell (15.84 cm^2)	BG
	Total EVA delaminate	D
	EVA delaminate by excluding busbar gridline	EVAD
	The area of the busbar gridline on the position of delaminate	$b_D g_D$
	Shading area on the cell	SA
	Exposure area on cell (non-shading area)	EA

3.5 The microstructure defection

In the investigation of microstructural defects in the cells, a representative cell on the severe degradation module was selected, using the scanning electron microscope (SEM) model: Leo 1455VP. The category of defect involves corrosion on the busbar, defect on the gridline, the defection of textured, and scarcity of composition crack on the cell. It is mandatory to fully analyze and explainable the cause and effect of defects and degradation models as predicting and comparing.

4. AN ELECTRICAL ANALYSIS

4.1 The IV-characteristic of the module's degradation

In this work, the module of both the natural degradation (ND) module and severe degradation (SD) module is selected, which is carried out to compare with the initial parameter's values of the I-V curves as illustrated in Fig.4. The results indicate that the average maximum power (P_m) of the ND module decreased by 46.56 W_p, and the degradation rate has reduced by 0.8% per year. The cause of the P_m of the SD module is 23.50 W_p and considerably decreased degradation rate by about 3.7% per year, the reduction is unusual. So, the other parameter is shown in Table 2. The degradation rate of the parameter of each module is represented in Table 3. Fig.4 found that the ND module will be the area under the curve more than the SD. When considering the resistance effect for the ND module found that a high R_{sh} amount of 288.39 Ω and Rs amount of 1.21 Ω the contrary SD module found that 20.52 Ω of R_{sh} and Rs 3.89 Ω. So, the severe degradation of the parasitic resistance is worse.

Table 2. The parameter of the I-V curves measured of PV module 53 Wp

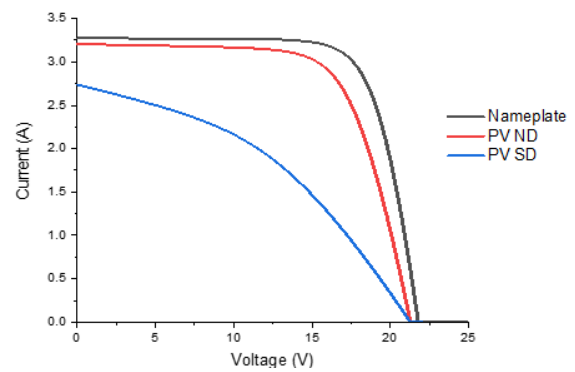| Parameter	PV Natural degradation	PV Severe degradation	Nameplate
I_{sc}, A	3.21	2.74	3.27
V_{oc}, V	21.30	21.30	21.80
I_{mp}, A	2.89	1.84	3.05
V_{mp}, V	16.11	12.79	17.40
P_m, W	46.56	23.50	53.00
R_{sh}, Ω	288.39	20.52	
R_s, Ω	1.21	3.89	
FF	0.68	0.40	

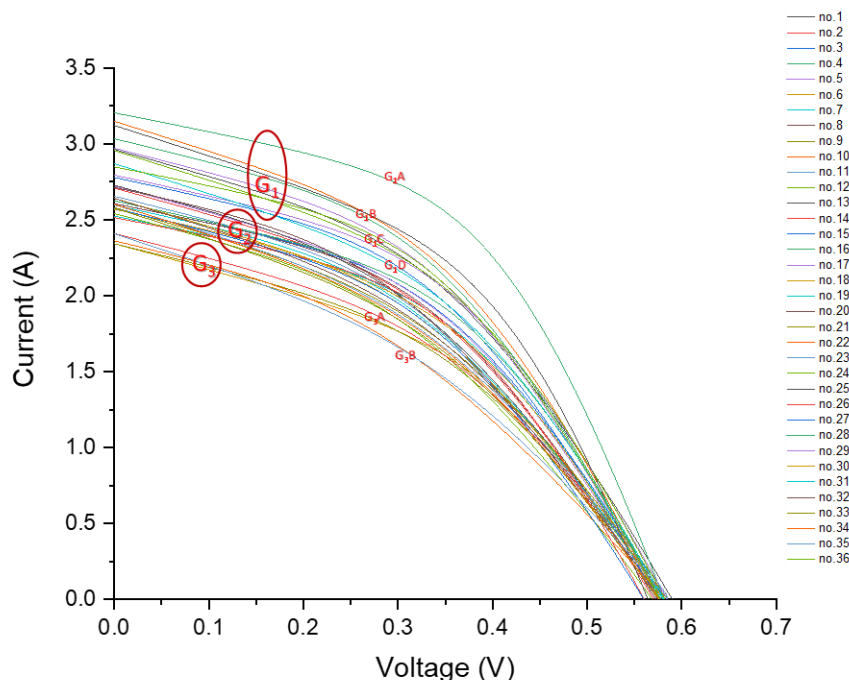

Fig.4. I-V characteristic of PV module 53 Wp.

Fig. 5. I-V curve of cell No.1-36 in the SD module.

Table 3. The degradation rate of the measured I-V curves of PV module 53 W$_p$

Degradation rate	PV Natural degradation (ND)	PV Severe degradation (SD)
$I_{sc\_degrade}$ (%)	1.96	16.08
$V_{oc\_degrade}$ (%)	2.29	2.31
$P_{m\_degrade}$ (%)	12.14	55.67

4.2 The IV-characteristic of the cells

The SD module representative was carried out to investigate degradation using the I-V curve at the standard testing condition (STC) of each cell. The detail of cells No.1-36 is illustrated as follows in Fig.5.

Table 4. The parameter of the measured I-V curves for each group in the SD module

Parameter	G$_1$	G$_2$	G$_3$
I_{sc}, (A)	2.98 $\pm$ 0.14	2.62 $\pm$ 0.06	2.38 $\pm$ 0.03
V_{oc}, (V)	0.58 $\pm$ 0.01	0.58 $\pm$ 0.01	0.58 $\pm$ 0.00
P_m, (W)	0.74 $\pm$ 0.06	0.61 $\pm$ 0.03	0.54 $\pm$ 0.02
I_{mp}, (A)	2.07 $\pm$ 0.13	1.77 $\pm$ 0.06	1.55 $\pm$ 0.03
V_{mp}, (V)	0.36 $\pm$ 0.01	0.35 $\pm$ 0.01	0.35 $\pm$ 0.01
FF	0.43 $\pm$ 0.02	0.41 $\pm$ 0.02	0.39 $\pm$ 0.02
R_s, (Ω)	0.0683 $\pm$ 0.0101	0.0883 $\pm$ 0.0106	0.1030 $\pm$ 0.0156
R_{sh}, (Ω)	0.53 $\pm$ 0.10	0.52 $\pm$ 0.10	0.46 $\pm$ 0.06
I_{pv}, (A)	3.37 $\pm$ 0.16	3.09 $\pm$ 0.15	2.93 $\pm$ 0.18
I_o, (A)	5.45 x 10^{-6} $\pm$ 2.56 x 10^{-6}	3.75 x 10^{-6} $\pm$ 2.72 x 10^{-6}	1.99 x 10^{-6} $\pm$ 1.29 x 10^{-6}
n	1.65 $\pm$ 0.04	1.60 $\pm$ 0.08	1.55 $\pm$ 0.09

The results show that there are different I_{sc}, consisting of the main groups of three. The high I_{sc} is a first group (G$_1$), and the I-V characteristic divide subgroup is 4. The G$_1$A (cell No.4) is a P_m value amount of 0.91 W, G$_1$B (cell No.22, 25, and 28) has an average value of Pm amount of 0.77 W, G$_1$C (cell No.1, 17, 24, 29, and 36) has the average value of P_m amount 0.72 W and G$_1$D (cell No.15 and 36) has the average value of P_m amount 0.68 W. The second is G$_2$ (cell No.2, 3, 5, 7, 8, 11, 12, 13, 16, 18, 19, 20, 21, 23, 26, 30, 32, and 33) of a medium I_{sc}, can see that the characteristic of I-V curve has the similar values. And the third is G$_3$ of a low I_{sc} when considering the curve of I-V characteristic of the graph found that the divided into 2 subgroups, including G$_3$A (cell No.6, 9 and 14) is Pm values amount 0.56 W, and G$_3$B (cell No.10 and 35) has the average value of P_m amount

0.51 W. In addition, the parameter values of G$_1$, G$_2$, and G$_3$ were showed in Table 4. So, the decrease of the IV curve of each group is caused by a loss of *FF*. These *FF* are decreased due to the attendance of parasitic resistive losses. Therefore, the *FF* is most imposed from the measured I-V curve and is described as the maximum power [13].

Fig.6 shows the I-V characteristic measurement of each cell (number of 36 cells) on the SD module combined and compared with the module measurement at STC, so the results indicated that the character of the line I-V curve is similar.
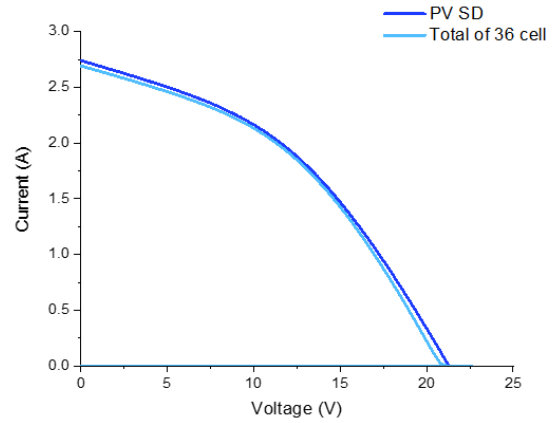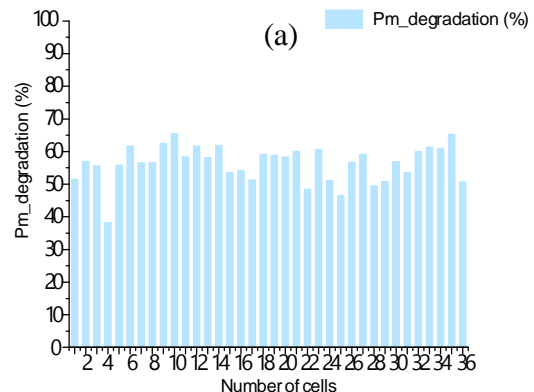

Fig. 6. Comparison of 36 cells of I-V curve from seriously degraded PV module.

4.3 The degradation rate analysis

The degradation rate analysis of each cell on the SD module found that the cell on the test module has a high %P$_{m\_degradation}$ and %FF$_{\_degradation}$. There are average values of about 52% and 43% respectively, shown in Fig.7(a) and (b). For the average value of %I$_{sc\_degradation}$, the amount is 15%, shown in Fig.7(c). While Fig.8(d) shows the % V$_{oc\_degradation}$ that each cell is not different. However, the degradation rate of cell No.4 found that %P$_{m\_degradation}$, %FF$_{\_degradation}$, and %I$_{sc\_degradation}$ are lower than others. So, it corresponds to the G$_1$A measurement of the IV curve of the previous section.
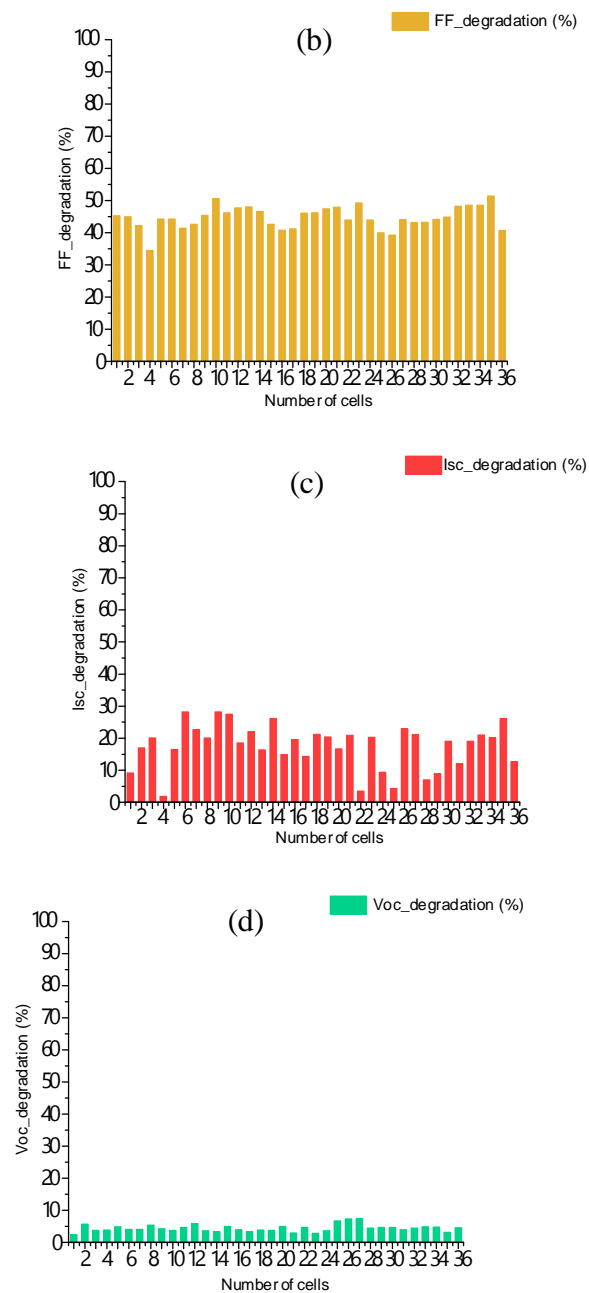
Fig.7. The degradation rate of P_m, FF, I_{sc}, and V_{oc}

and (b), respectively. And an increased value of %$P_{m\_degradation}$ and %$FF_{\_degradation}$ is caused by high R_s and low R_{sh} illustrates in Fig.9(c) and (d), respectively.
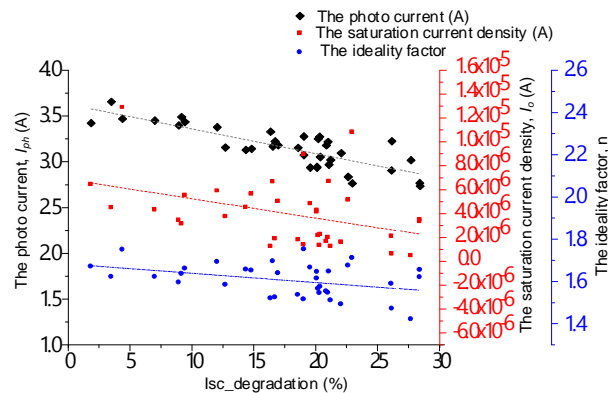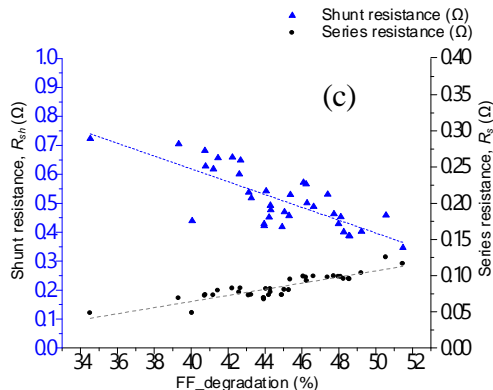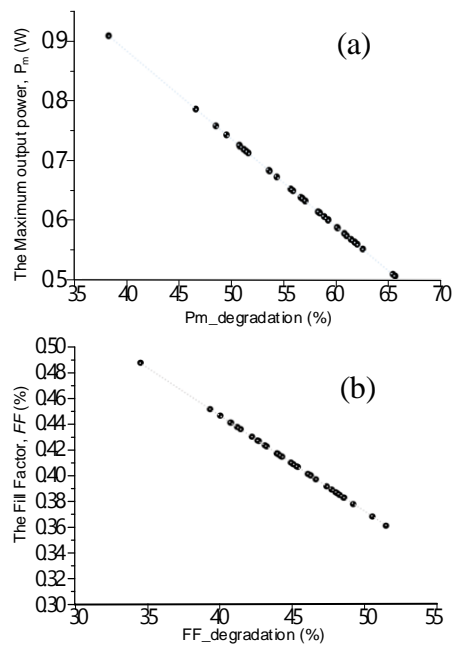

Fig.8. The relationship between the photocurrent, saturation current density, and ideality factor with the degradation rate of I_{sc}

In addition, our analysis of the relationship between the Isc degradation rate with the parasitic parameter found that the photocurrent (I_{ph}), the saturation current density (I_0), and the ideality factor (n) have a downward trend according to an increase of I_{sc} degradation rate shown in Fig.8. Therefore, the parasitic parameters of I_{ph}, I_0, and n correspond to %$I_{sc\_degradation}$ in terms of the deterioration rate increases the parasitic parameter decreases.

The value of percentage maximum power generation degradation (%$P_{m\_degradation}$) and percentage fill factor degradation (%$FF_{\_degradation}$) was an increase when a decreased value of the P_m and FF showed that in Fig.9(a)
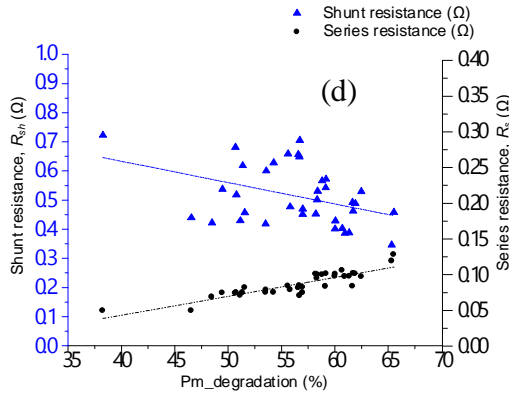
Fig.9. (a) The correlation between the degradation rate of P_m with the maximum output power. (b) The correlation between the degradation rate of FF with the fill factor. (c) The correlation between the shunt resistance and series resistance with the degradation rate of P_m. (d) The correlation between the shunt resistance and series resistance with the degradation rate of FF.

4.4 The correlation of parasitic effect

The correlation of 5 parameters including R_s, R_{sh}, I_{ph}, I_0, and n shown in the details following Fig.10 illustrates the reliance of the empirically predicted values of n and I_0 on different I_{sc} under the same irradiation conditions. The n and I_0 values are represented of the processes of recombination in PV cells. While the variation of n and I_0 values with I_{sc} were similar. The increased value of n and I_0 increasing I_{sc} cause of increasing Auger recombination in the bulk, front, and rear emitters, although under common irradiation conditions, Auger recombination is autonomous of the injection level. Moreover, under normal irradiation conditions found that decreased value both n and I_0 due to reducing recombination in the space charge region were reported. At a low irradiation intensity, the recombination in the space charge region was dominated, resulting in a higher n value. With increasing irradiation intensity can generate more charge carriers in the bulk region, increasing the rate of recombination in the bulk, and decreasing the amount of charge carriers in the space charge region [14]. The relationship between the I_0 and I_{sc} indicate that the variation of I_{ph} of PV cell with I_{sc}. Current parameters show linearly relation and increase with increasing I_{sc}. The theoretically and experimentally of this result has agreeable to [15]. Accordingly, there has a concurrence of scientists about the photocurrent of short circuit current. The I_{ph} values are conjugate to I_{sc} or agreeable the same.

Reduction of the effective of the solar cell due to disappearing power in the resistance is namely resistive effect. The normal resistance is R_s and R_{sh}, shown in Fig.11 that the variation in the R_s and R_{sh} values with maximum power. The maximum power increase found that increased R_{sh}, and in the other decreased R_s. Explainable by the maneuver of current through the p-n junction of the solar cell, the resistance of contact between the metal surface and

the silicon material, and the top and rear at metal contacts resistance [16]. For, the relationship between maximum power and the R_{sh} increase. While low R_{sh} effects power losses in solar cells that delivering an alternate current path for the light-generated current. An avocation decreases the amount of current flow throughout the p-n junction in the solar cell and reduces the voltage. The result of the R_{sh} is seriously drastic at low light levels because of the less light-generated current [17].
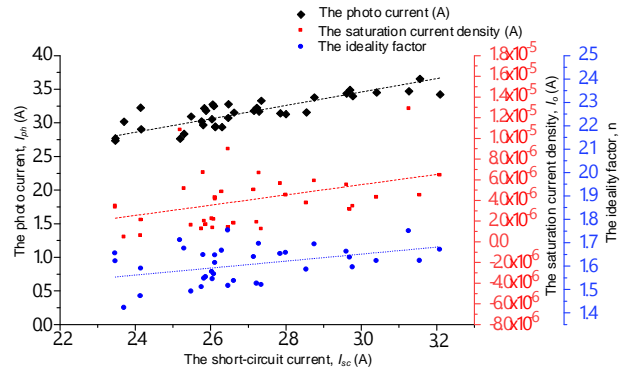

Fig.10. The relationship between the photo current, saturation current density and ideality factor with the short circuit current.
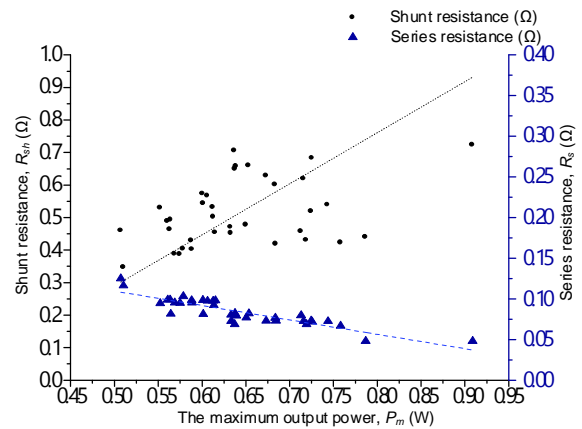

Fig. 11. The relationship between resistance with the maximum output power.

The fill factor losses due to R_s and R_{sh} are shown in Fig.12. Increasing R_s decreases the fill factor of the cell. Meanwhile, the high R_s is due to their field exposure of more than 15 years and climate, so it is generally very hot and humid with torrential rains. Because of the humidity condition that the dampness enters throughout the back sheet of the modules and trundles into the solder joints resulting in decay that diminishes the grid line and the busbar. This mechanism of electrons is generated in the cell clamber to a ribbon but diminishes and long direction to get relocated thus increasing the R_s [18]. The relationship between R_{sh} with FF is direct variation.
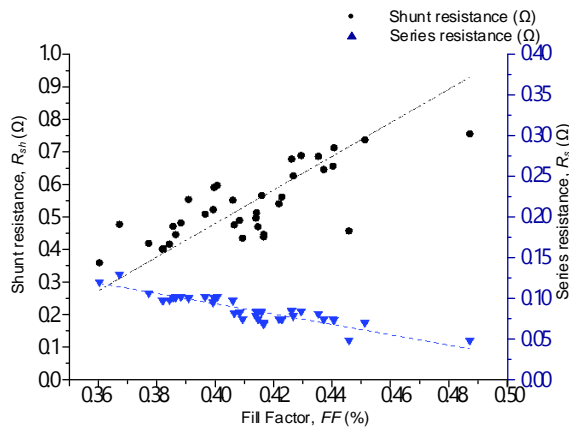
Fig.12. The relationship between resistance with FF

Fig.13 showed the responsibility of the fill factor on the ideality factor. The evident increase of the fill factor that increases the values of the diode ideality factor [19] is shown.
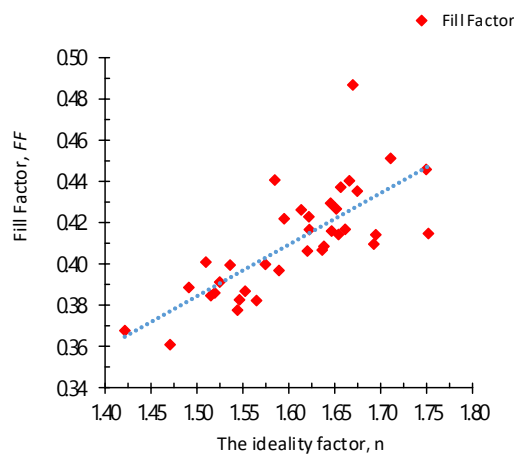

Fig.13. Correlation between *FF* and ideality factor

5. PHYSICS ANALYSIS

5.1 The EVA delamination analysis

Fig. 14 and 15 shown that although the delamination of EVA on the top surface of the solar cell, I_{sc} and Pm are unaffected EVA delamination. That evident the light can also be reach into the cell. The representative EVA delamination of each cell in the SD module is an exhibit in Fig.16. However, as previously reported by other researchers found that the EVA delaminate effect on the electrical characteristic. Because of the EVA delaminate effect to the exposure area loss, and cause of generating electricity has decreased. The light input to the cell reduces due to delaminated area, which resulting the short-circuit current of cell decrease [20]. Therefore, in this research, the alike IV-characteristic of the group of G_2 was studied, which studied in the IV-characteristic of the cells the EVA-delaminate on cell effect to decrease of I_{sc}

including cell No. 19, 30, and 5, respectively are selected according of the EVA delaminate area are descending. When the results of I_{sc} were considered as per a high of EVA delaminate effect to decrease of I_{sc} shows that in Fig.17.
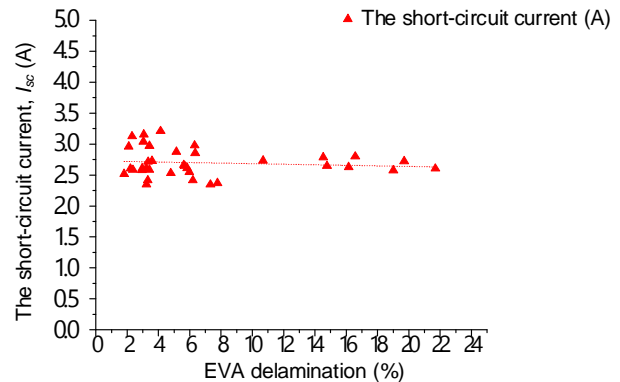

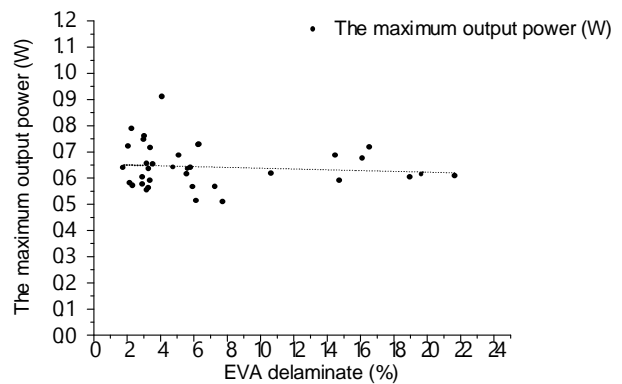**Fig.14. The EVA delamination and *I_{sc}* of each cell.**

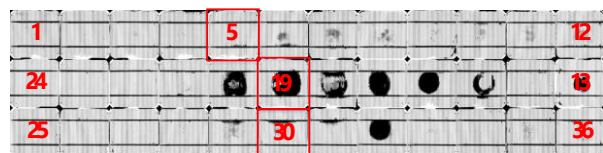**Fig.15. The EVA delaminate and *P_m* of each cell.**

Fig.16. Effect of EVA delaminate area on the cell.

For the group of EVA delamination of non-effect, in this research. It might be caused by the occurrence of parasitic resistance of the defect on the microstructural of the cell. There is result to an addition of series resistance and a reduction of current. So, discussed the result of detailed studies, are shown in the next section.

5.2 The microstructural analysis

The microstructure defect investigation. the electrical cell in the group of G_3 is selected, which was studied in the previse section. Due to the group effect of a high R_s and R_{sh} cells No.6, 9, 10, 14, and 35. A diagnostic of degradation

consisting of corrosion on busbar, defect of gridline, defect of textured, and defect of composition rupture on the cell was analyzed. The effect of resistance loss, shows in the details as follows:
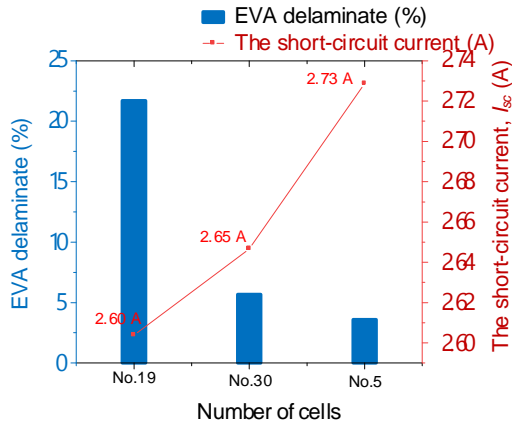

Fig. 17. Effect of EVA delaminate VS short circuit current.

5.3 Corrosion on busbar

The defect on the busbar region found that corrosion of green and corrosion of black may be deteriorate of copper compound such as malachite ($Cu_2(OH)2CO_3$) and copper (II) (oxide Cu_2O) [21,22]. Moreover the decay on the busbar cause the degradation rate is higher. [7]. As a result of the mechanism of galvanic corrosion caused by a reaction with water. The corrosion mechanism occurs at the interface between Cu-Sn-Pb alloy of solder plated ribbon and Ag. Metals which has lower voltage potential referring to as oblation metals, can normally abrade at greater rates than higher voltage potential metals [23]. Fig.18(a) shows the green patina area when analysis by SEM image of 25X and 500X found that the defect of the microstructural, shown in Fig.18(b) and (c) respectively. It might be caused by corrosion of malachite ($Cu_2(OH)2CO_3$) [21]. For, Fig.18(d) shows the structure of the black area, when analysis by the SEM image of 25X and 500X found that the defect of microstructural by oxide, shown in Fig.18(e) and (f) respectively. It may be caused by corrosion of Copper (II) oxide (CuO) appears on the surface of copper, it's shown in corrosion of cuprite [24]. Fig.18(g) shown the region of non-defect on the busbar and Fig.18(h) shown the SEM image at 500X found that this region is non-appearance of the defect.

5.4 Micro crack on busbar

Fig.19 (a) shows a cross-sectional image for a defect in the busbar region, found that the micro-crack near the busbar region between the cell and EVA sheet, there is an effect increased the shading area generated on the cell caused by the light shone through difficulty [25]. In addition, the micro-crack of the busbar affects the electric current flowing through the inconvenience and a decrease in power. Fig.21(b) found that the defect of the micro-crack between the cell and the busbar may cause by the throw of flowing

the cell that can not deliver electricity to the wires connected. The flow resistance of electricity affects to increase in series resistance and occurs a reduction of power [26]. Fig.21(c) is a cross-sectional image of the region of non-defect near the busbar found smooth and quite complete.
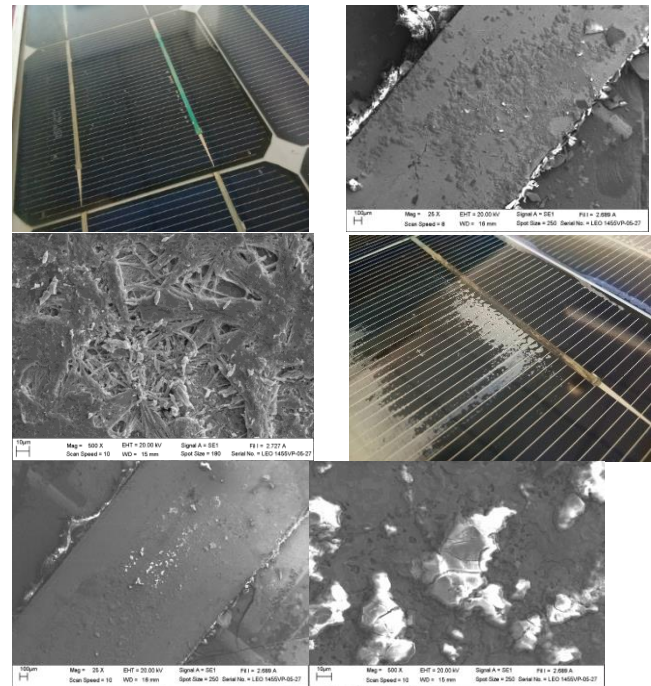

Fig.18. (a) shown the green patina area, (b) SEM image of 25X, (c) SEM image of 500X, (d) show the structure of the black area, (e) SEM image of 25X, (f) SEM image of 500X .
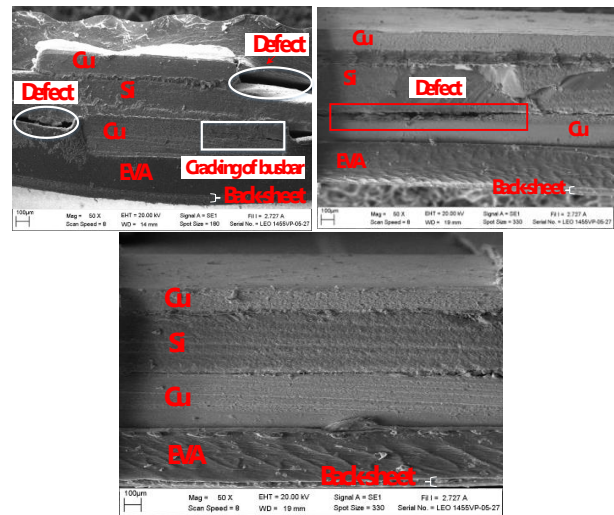

Fig. 19. The result of a defect of near busbar (a) micro-crack of busbar (b) micro-crack of cell and busbar (c) region of non-defect.

6. CONCLUSIONS

In this study, the main conclusions can be summarized as follows. The ND module has reduced 0.8% per year of Pm compare with the nameplate and the PV SD module found that a decrease of Pm of the down nameplate is about 3.7% per year. The result of the IV-curve measurement of each cell found that the group of reducing I_{sc} and P_m causes a high R_s and low R_{sh} which affects a decrease in FF. Each cell on the module effect a high the %$P_{m\_degradation}$ and %$FF_{degradation}$. The %$P_{m\_degradation}$ and %$FF_{degradation}$ cause high R_s and low R_{sh}. The %$I_{m\_degradation}$ is an increase when a reduction of I_{sc}, by the value of I_{ph} is a direct variation according to the value of I_{sc}. The I_0 and n have a downward trend according to an increase of the %$I_{sc\_degradation}$. The current generation behavior in the PV cell is uneffect from the EVA delamination. The investigations of microstructural defects found corrosion on the busbar and the micro-crack between the cell and busbar expected the cause a reduction in power generation.

ACKNOWLEDGMENT

REFERENCES

[1] Abdullatif, m. (October 15, 2016). Renewable Energy - solar energy. https://www.linkedin.com/pulse/ renewable-energy-solar-mohamed-abdullatif/

[2] Mohtasham, J. (2015). Review Article-Renewable Energies. Energy Procedia 74, 1289 – 1297.

[3] Bouraiou, A., Hamouda, M., Chaker, A., Mostefaoui, M., Lachtar, S., Sadok, M., Boutasseta, N., Othmani, M. and Issam, A. (2015). Analysis and evaluation of the impact of climatic conditions on the photovoltaic modules performance in the desert environ. Energy Conversion and Management 106, 1345–1355.

[4] Quansah, D.A., Adaramola, M.S., Takyi, G. and Edwin, I.A. (2017). Reliability and Degradation of Solar PV Modules-Case Study of 19-Year-Old Polycrystalline Modules in Ghana. Technologies 5, 1-18.

[5] Bandou, F., Arab, A.H., Belkaid, M.S., Logerais, P.O., Riou, O. and Charki, A.. (2015). Evaluation performance of photovoltaic modules after a long time operation in Saharan environment. International journal of hydrogen energy 40, 13839-13848.

[6] Köntges, M., Kurtz, S., Packard, C., Jahn, U., Berger, K.A., Kato, K., Friesen, T., Liu, H. and Iseghem, M.V. (2014). Review of Failures of Photovoltaic Modules. IEA PVPS Task 13.

[7] Rajput, P., Tiwari, G.N., Sastry, O.S., Bora, B. and Sharma, V. (2016). Degradation of mono-crystalline photovoltaic modules after 22 years of outdoor exposure in the composite climate of India. Solar Energy 135, 786–795.

[8] Sharma, V. and Chandel, S.S. (2016). A novel study for determining early life degradation of multi-crystalline-silicon photovoltaic modules observed in western Himalayan Indian climatic conditions. Solar Energy 134, 32–44.

[9] Meyer, S., Timmel, S., Richter, S., Werner, M., Gläser, M., Swatek, S., Braun, U. and Hagendorf, C. (2014). Silver nanoparticles cause snail trails in photovoltaic modules. Solar Energy Materials and Solar Cells 121, 171-175.

[10] Wohlgemuth, J.H. (2012). Standards for PV Modules and Components – Recent Developments and Challenges. The 27th European Photovoltaic Solar Energy Conference and Exhibition, 24-28.

[11] Bai, J., SLiu, S., Hao, Y., Zhang, Z., Jiang, M. and Zhang, Y. (2014). Development of a new compound method to extract the five parameters of PV modules. Energy Conversion and Management 79, 294–303.

[12] Chandel, S.S. and Sharma, V. (2013). Performance and degradation analysis for long term reliability of solar photovoltaic systems: A review. Renewable and Sustainable Energy Reviews 27, 753-767.

[13] PV education. (2019). Fill Factor. https://www. pveducation.org/pvcdrom/solar-cell-operation/fill-factor

[14] Khan, F., Baek, S.H. and Kim, J.H. (2014). Intensity dependency of photovoltaic cell parameters under high illumination conditions: An analysis. Applied Energy 133, 356–362.

[15] Cuce, E., Cuce, M.C. and Bali, T. (2013). An experimental analysis of illumination intensity and temperature dependency of photovoltaic cell parameters. Applied Energy 111, 374-382.

[16] [16] PV education. (2019). Series Resistance. https://www. pveducation.org/pvcdrom/solar-cell-operation/series-resistance

[17] PV education. (2019). Shunt Resistance. https://www. pveducation.org/pvcdrom/solar-cell-operation/shunt-resistance

[18] Tummala, A. (2016). Effect of Series Resistance Increase on Fill Factor of PV Cells Extracted from Field Aged Modules of Different Climates. Arizona State University.

[19] Elias, B.H. (2014). Modeling and Simulation of Photovoltaic Module Considering an Ideal Solar Cell. International Journal of Advanced Research in Physical Science (IJARPS) 1, 9-18.

[20] Chattopadhyay, S., Dubey, R., Kuthanazhi, V., John, J.J., Solanki, C.S., Kottantharayil, A., Arora, B.M., Narasimhan, K. L., Kuber, V., Vasi, J., Kumar, A. and Sastry, O. S. (2014). Visual Degradation in Field-Aged Crystalline Silicon PV Modules in India and Correlation With Electrical Degradation. IEEE Journal of Photovoltaics 4, 1470-1476.

[21] Kareem, K., Sultan, S. and He, L. (2016). Fabrication, microstructure and corrosive behavior of different metallographic tin-leaded bronze alloys part II: Chemical corrosive behavior and patina of tin-leaded bronze alloys. Materials Chemistry and Physics 169, 158-172.

[22] Siatou, A., Charalambous, D., Argyropoulos, V. and Pouli, P. (2006). A Comprehensive Study for the Laser Cleaning of Corrosion Layers due to Environmental Pollution for Metal Objects of Cultural Value: Preliminary Studies on Artificially Corroded Coupons. Laser Chemistry, 1-7.

[23] Kim, J.H., Park, J., Kim, D. and Park, N. (2014). Study on Mitigation Method of Solder Corrosion for Crystalline Silicon Photovoltaic Modules. International Journal of Photoenergy, 1-9.

[24] Osayemwenre, G.O., Meyer, E.L. and Mamphweli, S.

(2015). Sem analysis as a diagnostic tool for photovoltaic cell degradation. Digest Journal of Nanomaterials and Biostructures, 479-487.

[25] Park, N.C., Jeong, J.S., Kang, B.J. and Kim, D.H. (2013). The effect of encapsulant discoloration and delamination on the electrical characteristics of photovoltaic module. Microelectronics Reliability 53, 1818-1822.

[26] Jeong, J.S., Park, N. and Han, C. (2012). Field failure mechanism study of solder interconnection for crystalline silicon photovoltaic m 2326-2330.